Lewy body disease primate model with α-synuclein propagation from the olfactory bulb

Masanori Sawamura, MD,[†1] Hirotaka Onoe, PhD,[†2] Hideo Tsukada, PhD,[3] Kaoru Isa,[4] Hodaka Yamakado, MD, PhD,[1] Shinya Okuda, MD, PhD,[1] Masashi Ikuno, MD, PhD,[1] Yusuke Hatanaka, PhD,[1] Shigeo Murayama, MD, PhD,[5, 6] Norihito Uemura, MD, PhD,*[1] Tadashi Isa, MD, PhD,[2, 4, 7] Ryosuke Takahashi, MD, PhD*[1]

[†]**These authors contributed equally to this work.**

Author affiliations:

1. Department of Neurology Graduate school of Medicine, Kyoto University, Kyoto, Japan,
2. Human Brain Research Center, Kyoto University Graduate School of Medicine, Kyoto, Japan,
3. Central Research Laboratory, Hamamatsu Photonics K.K., Shizuoka, Japan,
4. Department of Physiology and Neurobiology, Kyoto University Graduate School of Medicine, Kyoto, Japan,
5. Department of Neuropathology (Brain Bank for Aging Research), Tokyo Metropolitan Geriatric Hospital & Institute of Gerontology, Tokyo, Japan.
6. Brain Bank for Neurodevelopmental, Neurological and Psychiatric Disorders, Molecular Research Center for Children's Mental Development, United Graduate School of Child Development, Osaka University, Osaka, Japan
7. Institute for the Advanced Study of Human Biology (WPI-ASHBi), Kyoto University, Kyoto, Japan

*Correspondence to: Norihito Uemura, MD, PhD & Ryosuke Takahashi, MD, PhD
Department of Neurology, Graduate school of Medicine, Kyoto University
54 Kawaharacho, Shogoin, Sakyo-ku Kyoto, 606-8507, JAPAN
E-mail: nuemura@kuhp.kyoto-u.ac.jp & ryosuket@kuhp.kyoto-u.ac.jp

Word count: Abstract 223 words, Text 3,621 words.

Running title: α-Synuclein propagation from the OB in primates

Relevant conflicts of interest/financial disclosures: Nothing to report

Funding agencies: This study was supported from the Ministry of Education, Culture, Sports, Science, and Technology (R.T., No. JP18K15450; Grant-in-Aid for Scientific Research (A), No. JP18H04041; Grant-in-Aid for Scientific Research on Innovative Areas, No. JP17H05698), the Integrated Neurotechnologies for Disease Studies (Brain/MINDS) from Japan Agency for Medical Research and Development, AMED (R.T., No. JP14dm0207020, JP19dm0207070, M.K., No. JP18dm0207024, H.O., No. JP20dm0207093, T.I., JP14dm0207020, S.M., JP18dm0107103), JSPS KAKENHI (M.S., No. JP19K23779, JP20K16493, S.M., No. JP16H06277). BBAR is funded by JSPS KAKENHI Grant No. JP16H06277, AMED under Grant No. JP18dm0107103 and National Center of Geriatric and Gerontology Fund.

Abstract

Background: Lewy body diseases (LBDs), which are pathologically defined as the presence of intraneuronal α-synuclein inclusions called Lewy bodies, encompass Parkinson's disease, Parkinson's disease with dementia (PDD), and dementia with Lewy bodies (DLB). Autopsy studies have revealed that the olfactory bulb is one of the regions where Lewy pathology develops and initiates its spread in the brain.

Objective: This study aims to clarify how Lewy pathology spreads from the olfactory bulb and affects brain functions using non-human primates.

Methods: We inoculated α-synuclein preformed fibrils (PFFs) into the unilateral olfactory bulbs of common marmosets (*Callithrix jacchus*) and performed pathological analyses, manganese-enhanced MRI (MEMRI), and ^{18}F-fluoro-2-deoxy-D-glucose PET (^{18}F-FDG-PET) up to 6 months postinoculation.

Results: Severe α-synuclein pathology was observed within the olfactory pathway and limbic system, while mild α-synuclein pathology was seen in a wide range of brain regions, including the substantia nigra pars compacta, locus coeruleus, and even dorsal motor nucleus of the vagus

nerve. The brain imaging analyses revealed reduction in volume of the olfactory bulb and progressive glucose hypometabolism in widespread brain regions, including the occipital lobe, and extended beyond the pathologically affected regions.

Conclusion: We generated a novel non-human primate LBD model with α-synuclein propagation from the olfactory bulb. This model suggests that α-synuclein propagation from the olfactory bulb is related to olfactory bulb atrophy and cerebral glucose hypometabolism in LBDs.

Keywords: α-synuclein; olfactory bulb; primate

Introduction

Lewy body disease (LBD) is an umbrella term of neurodegenerative diseases which are pathologically characterized by the presence of intraneuronal α-synuclein (α-Syn) inclusions called Lewy bodies (LBs).[1] LBDs are comprised of incidental Lewy bodies (ILBs), Parkinson's disease (PD), PD with dementia (PDD), and dementia with Lewy bodies (DLB).[1,2] PD is the second most common neurodegenerative disorder after Alzheimer's disease.[3] Its pathological hallmarks include LBs and the loss of dopaminergic neurons in the substantia nigra pars compacta (SNc).[4] Clinically, PD has been characterized by classical motor symptoms and various non-motor symptoms.[5] It has been reported that 83% of patients with PD who survive 20 years after the onset develop dementia; this condition is called PDD.[6] In contrast, if the development of dementia precedes or occurs within one year of the onset of parkinsonism, the patients are diagnosed as DLB.[1]

Based on the systematic postmortem analyses of cases with ILBs and patients with PD, Braak et al.[7,8] established a staging system for PD and hypothesized that Lewy pathology initially develops in the olfactory bulb (OB) and the dorsal motor nucleus of the vagus nerve (dmX) and/or gastrointestinal tract, subsequently spreading in the brain in a stereotypic manner. Therefore, it is important to clarify how the initial OB pathology progresses and contributes to

neurological deficits in LBDs.

Recent accumulating evidence suggests that α-Syn in LBDs can spread like prion in the brain.[9-13] It has been also shown that inoculation of α-Syn preformed fibrils (PFFs) into the mouse OB induced propagation of α-Syn pathology mainly along the olfactory pathway and the limbic system, eventually reaching the SNc and the locus coeruleus (LC).[14-17] Although these studies enhanced our understanding of progression of the Lewy pathology from the OB, it remains unclear how applicable these results are to human LBDs, because of the considerable differences in the brain structure and olfactory system between rodents and primates.[18,19]

A small new world primate, common marmoset (*Callithrix jacchus*) has been increasingly used as an experimental non-human primate (NHP).[20] Marmosets are easier to handle than macaque monkeys due to their small body size and relatively short maturation time.[18] In addition, their social cognitive abilities, highly developed brain structure, and suitability for transgenesis and imaging analyses make marmosets a useful animal model for neuroscience and neurological/psychiatric disease research.[18,21] Moreover, striatal inoculation with α-Syn PFFs in marmosets was reported to induce the degeneration of dopaminergic neurons in the SNc, indicating their potential as an animal model for LBDs research.[22]

In this study, we hypothesized that α-Syn pathology spreads from the OB through neruroanatomical routes within primate brains, affecting their neurological functions. To this end, we applied OB injections of α-Syn PFFs to marmosets and analyzed them by pathological and imaging analyses. To the best of our knowledge, this is the first study describing the propagation of α-Syn pathology via the olfactory system in NHPs, which provides several important implications regarding the initiation and progression of LBDs.

Materials and methods

Preparation of marmoset α-Syn expressing plasmid

Details are provided in Supplementary Methods.

Preparation of recombinant α-Syn and PFFs

Recombinant human α-Syn (h-α-Syn) and mar-α-Syn monomer and PFFs were prepared and characterized as described previously.[15,23] Details are provided in the Supplementary Methods.

In vitro α-Syn fibrillization assay

Details are provided in the Supplementary Methods.

Animals

Four marmosets were used for α-Syn PFFs inoculation into the unilateral OB. The experimental information was shown in Supplementary Table S1. Details are provided in the Supplementary Methods.

Inoculation with α-Syn PFFs into the OB

We inoculated 0.8 μl of 4 mg/ml α-Syn PFFs into the two sites of the unilateral OB in four marmosets. The same volume of PBS was also injected into the contralateral OB. Details are provided in the Supplementary Methods.

Preparation of histological analysis for the marmosets

Details are provided in Supplementary Methods.

Human brain samples

We compared α-Syn pathology of the marmosets with that of patients with PD. The human brains of two patients with PD (Patient 1 and Patient 2) and one age- and sex-matched healthy control subject (Control 1) were obtained from the Brain Bank for Aging Research (BBAR), whose activity was approved by TMGHIG IRB. These brains were examined using the BBAR protocol.[24] Briefly, these brains were sliced into 8 mm slabs, which were fixed for 48 hrs in 4% (w/v) PFA and subsequently embedded in paraffin. Immunostaining was performed with an automated immunostainer (Ventana XT DISCOVERY; Ventana, Tucson,

AZ, USA). Braak PD stage (Braak PD), BBAR LB stage (BBAR LB), Senile plaque, Braak neurofibrillary tangle (NFT) stage (silver staining and AT8) were determined as previously described.[24]

Immunohistostaining and Thioflavin S staining

Details are provided in Supplementary Methods.

Heatmap and scoring of p-α-Syn pathology

We assessed the p-α-Syn pathology density in various brain regions using quantitative methods modified to generate a heatmap from a previous report.[17] Also, we assessed the severity of p-α-Syn pathology in a semi-quantitative way, based on the previous reports,[16,17] in the same coronal sections as those shown by positron emission tomography (PET) images (FIG. 5). Details are provided in Supplementary Methods.

Manganese-Enhanced MRI (MEMRI)

We performed Manganese-Enhanced MRI on four unilaterally PFFs-inoculated marmosets at 3 mpi (H81, H82, I5937, and I5924). Details are provided in the Supplementary Methods.

PET imaging and data analysis

We performed ^{18}F-FDG-PET on H81 at 3 mpi and I5937 at 6 mpi, and analyzed these PET data. To identify the changes in rCGU after the inoculation, original ^{18}F-FDG-PET images were flipped horizontally, and were subjected to a voxel-based subtraction from the flipped images comparing the affected and unaffected brain hemispheres. Details are provided in the Supplementary Methods.

Statistical analysis

An unpaired *t*-test or paired *t*-test was used. Statistical calculations were performed

with GraphPad Prism Software, Version 5.0.

Data availability

The authors confirm that the data supporting the findings of this study are available within the article and its supplementary materials.

Results

Inoculation of marmoset α-Syn PFFs into the marmoset OB

Marmosets possess the *SNCA* gene (https://useast.ensembl.org/Callithrix_jacchus/Info/Index), and four amino acid residues differ between the mar-α-Syn and h-α-Syn (Supplementary Figure S1A). Since it was reported that cross-seeding between mouse α-Syn and h-α-Syn is less efficient than homologous seeding,[25] we examined which α-Syn PFFs, mar-α-Syn or h-α-Syn PFFs, more efficiently induce fibrilization of mar-α-Syn monomer *in vitro*. We generated recombinant mar-α-Syn monomer and analyzed the kinetics of fibrilization of mar-α-Syn monomer seeded with mar- or h-α-Syn PFFs by *in vitro* α-Syn fibrillization assay. First, we agitated mar-α-Syn monomer alone to generate mar-α-Syn PFFs. The smear band in CBB staining and the high signal intensity of ThT fluorescence indicated α-Syn polymerization and the presence of β-sheet-rich structures, respectively (Supplementary Figure S1B and C). *In vitro* α-Syn fibrillization assay revealed faster fibrilization of mar-α-Syn monomer in the presence of mar-α-Syn PFFs than in the presence of h-α-Syn PFFs (Supplementary Figure S1D). We therefore used mar-α-Syn PFFs for the inoculation experiments in marmosets, assuming that mar-α-Syn PFFs induce more severe α-Syn pathology in marmosets than h-α-Syn PFFs. We examined the position of the OB in marmosets with CT/MRI fusion images (Supplementary Figure S1E), which confirmed the surgical accessibility of the OB before the operation in the first marmoset. The marmoset OB were located anterior to the frontal lobe, allowing us to reach them after the removal of the frontal skull (Supplementary Figure S1F). α-Syn PFFs were stereotactically inoculated into the OB with a glass capillary (Supplementary Figure S1G).

Propagation of α-Syn pathology induced by α-Syn PFFs inoculation into the unilateral OB.

A previous study has shown that the inoculation of α-Syn PFFs into the marmoset striatum induced the widespread propagation of α-Syn pathology at 3 mpi.[26] Therefore, we sacrificed the unilaterally PFFs-inoculated marmosets at 3 and at 6 mpi for pathological analyses. Immunostaining to detect p-α-Syn, a marker of pathological α-Syn in Lewy pathology, revealed abundant α-Syn pathology in the ipsilateral OB at 3 mpi (FIG. 1A–E). P-α-Syn-positive LB-like inclusions were observed in mitral cells, periglomerular cells, and granular cells (FIG. 1C–E), while p-α-Syn-positive dot-like depositions were observed in the glomeruli (FIG. 1B). Sparse p-α-Syn-positive inclusions were observed on the contralateral side (FIG. 1F). P-α-Syn-positive inclusions were more abundant in the central area than in the peripheral area of the granular cell layer (FIG. 1A). A few p-α-Syn-positive inclusions were observed in the mitral cells and the periglomerular cells, but many p-α-Syn-positive inclusions were in the granular cells (FIG. 1A).

In the OB of patients with PD, p-α-Syn-positive cytoplasmic inclusions were frequently observed in granular cells, followed by mitral cells, tufted cells, and periglomerular cells (FIG. 1H, I, K–N). In addition, dot-like p-α-Syn-positive depositions were observed in the glomeruli (FIG. 1K). No p-α-Syn pathology was observed in the OB of the age-matched control subject (FIG. 1J). The detailed pathological stages and clinical information were shown in Supplementary Table S2. Overall, the pathological findings in the OB of the marmosets inoculated with α-Syn PFFs resembled those seen in the subjects with PD.

Abundant α-Syn pathology was also observed along the olfactory pathway on the ipsilateral side including the amygdala and piriform cortex (FIG. 2A), indicating that the pathology spreads to anatomically connected regions with the OB in NHPs. Of note, because no p-α-Syn pathology was seen in the superficial layers of the OB or other brain regions, even in the adjacent to OB, it is unlikely that α-Syn PFFs diffused through the subarachnoid space and then were taken up by distant brain regions. LB-like and Lewy neurite-like p-α-Syn

depositions were observed in these regions showing abundant α-Syn pathology (FIG. 2B). These structures were also detectable with other p-α-Syn antibodies (FIG. 2C and D) and ThS, and were immunopositive for p62 and ubiquitin, similarly to LBs in LBDs (FIG. 2E–M). Moreover, we treated these brain sections with proteinase K (ProK), as abnormally aggregated α-Syn in LBs is known to be ProK-resistant. Whereas ProK treatment diminished the background of p-α-Syn staining, ProK resistant p-α-Syn positive aggregates were still abundant (Supplementary Figure S2). In addition, they were exclusively observed in neurons, not in astrocytes, microglia, or oligodendrocytes (FIG. 2N–Q). There were no obvious changes in terms of glial activation in the piriform cortex between ipsilateral and contralateral sides (Supplementary Figure S3), which is consistent with a previous report.[16] Considerable α-Syn pathology was also observed in the limbic system including the hippocampus, where α-Syn inclusions were predominantly seen in the dentate gyrus and CA1 (FIG. 2R–V). No p-α-Syn pathology was observed in a normal control marmoset (FIG. 2W).

α-Syn pathology throughout the brains is shown by representative images (FIG. 3A, B) and a heatmap quantifying p-α-Syn-positive areas (FIG. 3C). At 3 mpi, we found abundant α-Syn pathology in the OB as well as in the olfactory cortices including the anterior olfactory nucleus (AON), olfactory tubercle, piriform cortex, amygdala, and entorhinal cortex on the ipsilateral side (FIG. 3A and C). α-Syn pathology was also observed beyond the olfactory pathway. α-Syn pathology spread to the hippocampus, nucleus accumbens (Acb), bed nucleus on the ipsilateral side at 3 mpi (FIG. 3A and C). Moreover, α-Syn pathology was seen in the SNc, LC, and pedunculopontine nucleus (PPN) (FIG. 3A and C).

At 6 mpi, more abundant α-Syn pathology was observed in the central amygdala nucleus, entorhinal cortex, CA1, and LC on the ipsilateral side (FIG. 3B and C). In contrast, the burden of α-Syn pathology was mildly decreased in the OB, AON, and piriform cortex (FIG. 3B and C). α-Syn pathology in the SNc was still mild at 6 mpi, and no obvious difference was observed between ipsilateral and contralateral sides (Supplementary Figure S4). In addition, we did not find apparent parkinsonism such as bradykinesia, tremor, or rigidity in this marmoset model. α-Syn pathology extended to the putamen on both sides, and in the entorhinal

cortex on the contralateral side (FIG. 3B). Furthermore, at 6 mpi, α-Syn pathology, albeit sparse, was observed even in the dmX (FIG. 3B and C). These results indicated that inoculation of the OB with α-Syn PFFs induced progressive α-Syn propagation along the olfactory pathway and limbic system, even extending to the brainstem nuclei. In addition, the heatmap shows similar distribution and amount of p-α-Syn pathology between the two marmosets at each time point, suggesting the reproducibility of α-Syn PFF-induced pathology in the marmosets (FIG. 3C).

OB atrophy in the unilaterally PFFs-inoculated marmosets

We assessed brain structures and activities using Manganese-Enhanced MRI (MEMRI). Since the manganese is known to be taken up by excitable neurons as a calcium (Ca^{2+}) analog, images obtained by this modality show high signal intensity in the brain.[27] Four unilaterally PFFs-inoculated marmosets were subjected to MEMRI analysis at 3 mpi to compare the volume and intensity of each brain region on the ipsilateral (PFFs-inoculated) side with those on the contralateral (PBS-inoculated) side (FIG. 4A–C and Supplementary Table S1). The volume and intensity ratio of the ipsilateral side to contralateral side was calculated within each marmoset (See Methods). The volume ratio showed significant atrophy in the ipsilateral OB (0.831±0.010, $p<0.01$) (FIG. 4D), but the intensity ratio did not differ significantly between the ipsilateral and contralateral sides (FIG. 4E). Moreover, ssDNA-positive cells were observed in the OB only on the ipsilateral side, indicating cell death (Supplementary FIG. S5).

Comparison of the p-α-Syn pathology and glucose hypometabolism in the unilaterally PFFs-inoculated marmosets

We performed ^{18}F-FDG-PET analyses on H81 at 3 mpi and on I5937 at 6 mpi before the sacrifice, then compared the pathological change with brain functional imaging (FIG. 5 and Supplementary Table S1). The pathological distribution is shown as a diagram of coronal sections illustrating semi-quantitative p-α-Syn-positive pathology (FIG. 5B and D). ^{18}F-FDG-PET images were flip-subtracted to reveal the difference between the ipsilateral and

contralateral sides (See Methods). ^{18}F-FDG-PET revealed hemispheric glucose hypometabolism on the ipsilateral side (FIG. 5A and C). The original data without flip-subtraction did not show apparent change on the ipsilateral side, while a decrease was seen on the contralateral side (Supplementary FIG. S6). Also, flip-subtracted images averaged across the 4 control marmosets showed only subtle differences between the hemispheres (0–0.1 SUV), which was performed for another project (data not shown).

At 3 mpi, glucose hypometabolism was seen in the Acb, AON, lateral geniculate nucleus (LGN) and the amygdala on the ipsilateral side (FIG. 5A). Moderate to severe p-α-Syn pathology was seen in the Acb, AON, central and basolateral amygdala nuclei, while no p-α-Syn pathology was observed in LGN (FIG. 5B). At 6 mpi, glucose hypometabolism was seen in the frontal lobe, extended amygdala, hypothalamus, thalamus, midbrain, optic radiation, and occipital lobe (primary visual area and visual area 4) on the ipsilateral side (FIG. 5C), while only mild or no pathology was seen in these brain regions (FIG. 5D). Because remarkable hypometabolism was seen in the visual pathway at 3 and 6 mpi, we looked for α-Syn pathology in the optic nerve but none was observed there (FIG. 5B and D, second panel from the left). The glucose hypometabolism was seen in widespread brain regions, including the occipital lobe and LGN, and extended beyond the pathologically affected regions (FIG. 5). The discrepancy between glucose hypometabolism and pathological changes was more widespread at 6 mpi than that at 3 mpi. In addition, artifacts were observed near the edge of the brain on the contralateral side. We found that the artifacts could be caused by high uptake into the temporal muscles (Supplementary FIG. S6).

Discussion

Although α-Syn PFF injection is artificial, this methodology can trigger α-Syn propagation from the injection site, providing unique opportunities to explore specific aspects of LBDs pathophysiology. Previous studies using NHPs have revealed that the inoculation of the striatum, SN, and gut with α-Syn PFFs or patient-derived LBs induced α-Syn pathology in

the brains.[13,22,28-30] However, no previous study has investigated α-Syn propagation from the OB in NHPs. This is partly because the OB in macaque monkeys is located underneath the frontal lobe and is quite difficult to approach with a stereotactic technique. In contrast, the OB in marmosets is located anterior to the frontal lobe and is easier to approach (Supplementary Figure S1E). In this study, we successfully inoculated α-Syn PFFs into the OB of marmosets and analyzed the progression of α-Syn pathology and functional changes by ^{18}F-FDG-PET.

The pathological analyses showed that the marmosets inoculated with α-Syn PFFs exhibited numerous cytosolic p-α-Syn inclusions in the OB, especially in the granular cell layer, and dot-like p-α-Syn depositions in the glomeruli. These distribution and morphological features were similar to those seen in the OB of patients with PD.[31] This marmoset model showed severe α-Syn pathology in the ipsilateral OB, AON, and piriform cortex at 3 mpi, but it was rather diminished at 6 mpi. The same observation was reported in previous studies of mice with α-Syn PFFs inoculation into the OB, which demonstrated that decrease in α-Syn pathology in the AON came from neuronal cell loss.[15,17] Indeed, the present study revealed OB atrophy by MRI and ssDNA-positive cells in the ipsilateral OB, which indicates neuronal cell loss in the OB on the PFF-injected side.

In addition to the olfactory system, the marmosets presented severe α-Syn pathology in the limbic system, such as the piriform cortex and amygdala. A previous report in mice showed that the central amygdala nucleus presented less α-Syn pathology than other amygdala nuclei.[16] However, this marmoset model presented the most prominent α-Syn pathology in central amygdala nucleus. Postmortem study of PD revealed that the α-Syn pathology was severe in the central and cortical nuclei of amygdala.[32] In this sense, our marmoset model may more faithfully recapitulate the amygdala pathology of PD. The α-Syn pathology spread further to the SNc and the lower brainstem nuclei at locations such as the PPN, LC and the dmX. The spread of α-Syn pathology to these nuclei may be explained by propagation through known neural circuits.[19,33,34] The olfactory bulb (OB) and anterior olfactory nucleus (AON) do not have direct connections with the central amygdala nucleus, but have indirect connections via the piriform cortex and entorhinal cortex.[35] Recently, non-motor symptoms such as hyposmia,

rapid eye movement sleep behavior disorder (RBD), and constipation have gained much attention as prodromal symptoms for PD and DLB.[36] The α-Syn pathology seen in the OB, olfactory cortex, and lower brainstem nuclei could be responsible for those symptoms in LBDs.[36,37] In this study, we analyzed young marmosets injected with α-PFFs, but aged marmosets would potentially show more widespread, robust α-Syn pathology based on a recent rodent report.[38]

We performed morphological and functional analyses of the marmoset brains after the inoculation with α-Syn PFFs. A volumetric analysis of MRI revealed a significant reduction in the OB volume ratio of the ipsilateral to the contralateral side in the inoculated marmosets. In line with this, the atrophy of OB was reported in patients with PD,[39] and the OB volume was inversely correlated with olfactory dysfunction.[39,40]

It is particularly noteworthy that this marmoset model showed glucose hypometabolism in the widespread brain regions including visual cortex. Glucose hypometabolism in the occipital lobe has been proposed as a supportive biomarker for DLB diagnosis,[41] and several studies have reported that glucose hypometabolism in brain regions such as the occipital lobe, parietal lobe, and cingulate cortex is a predictive marker of cognitive dysfunction in patients with PD.[42,43] Moreover, two longitudinal studies have demonstrated that hyposmia is a predictive marker for conversion from PD to PDD.[44,45] PD patients with hyposmia had an 18.7-fold increase in the risk of dementia within the three-year observation period.[44] PD patients with hyposmia (42/91, 46%) at baseline developed dementia compared to normosmic patients (7/34, 21%) during the follow up period of ten years.[45] High prevalence of olfactory dysfunction has been also reported in DLB compared to AD.[46] All these findings suggest a close association between α-Syn propagation from the OB and cognitive dysfunction in LBDs, which was supported by the present study.

In addition, the glucose hypometabolism of this marmoset model was widespread, extending beyond the pathologically affected regions. This discrepancy may be explained by neurotoxicity of smaller forms of α-Syn fibrillization, i.e. oligomers, which are not detected by conventional immunohistochemistry[47], or remote effects as perturbation of projections from

cardinal nuclei such as nucleus basalis of Meynert or LC. Note that we applied flip-subtraction to minimize the effects of individual differences due to difficulty in getting a large number of animals. α-Syn pathology on the contralateral side possibly underestimated the detection of hypometabolism in the method, while the hypometabolism on the ipsilateral side was also seen in the original data without flip-subtraction (Supplementary FIG. S6).

There are several limitations in this study. First, the present study analyzed a small number of marmosets, including 2 marmosets receiving ^{18}F-FDG-PET imaging, up to 6 mpi, relatively short incubation time. This limitation comes from the preliminary nature of this study. Second, this study lacks detailed behavior analysis regarding hyposmia, cognitive dysfunction, and motor symptoms. We are currently working on the establishment of those tests for a future study. Also, we have to consider longer incubation on a sufficient number of animals to examine the relationship between imaging abnormalities and behavioral changes in a future study. Lastly, we cannot completely rule out the effects of bacteria-derived contaminants in α-Syn PFFs on this marmoset model. However, we did not see obvious microglial activation or reactive astrocytes on the PFF-injected side compared to the PBS-injected side, which could be caused by the contaminants like lipopolysaccharide (Supplementary FIG. S3). Therefore, we presume that the contaminants did not have obvious effects in this marmoset model.

In conclusion, this study revealed that the α-Syn PFFs inoculation into the OB induces the α-Syn propagation to anatomically connected brain regions, OB atrophy, and widespread cerebral glucose hypometabolism, and the pathological mechanisms underlying the association of olfactory dysfunction with development of cognitive dysfunction in PD.[44,45] These findings may lead to future development of biomarkers predicting cognitive dysfunction and new therapies preventing it in LBDs.

Acknowledgements

We thank Shuichi Matsuzawa, Maiko Uemura, Takashi Ayaki, Seiji Kaji, and Chen Chih-Yang for insightful suggestions and kind support. We thank Jiro Yamashita for animal care, Norihiro Harada, Shingo Nishiyama, Hiroyuki Ohba, Takeharu Kakiuchi, and Kayo Onoe for PET data

acquisition and analyses, and Kei Kubota and Jun Takahashi for MRI acquisition. We are grateful to Denis Matrov for providing marmoset brain tissue. We thank Hirokazu Hirai of Bioresource Center, Gunma University Graduate School of Medicine for supplying marmosets. We appreciate Yasuko Matsuzawa and Maho Morishima supporting the paperwork.

Author roles

Design, H.O., R.T., T.I., and N.U.; Execution, M.S., K.I., and H.O.; Analysis, S.M., H.Y., S.O., M.I., and Y.H.; Writing, M.S., H.O., H.T. and N.U.; Editing of final version of the manuscript, M.S., N.U., and R.T.

Financial Disclosures of all authors (for the preceding 12 months)

M.S. received grants from JSPS. M.I. received grants from JSPS. H.Y. received grants from JSPS and JST. S.M. received grants from JSPS and AMED. H.O. received grants from AMED. T.I. received grants from AMED. R.T. received consultancies from KAN Research Institute, Inc.; grants/research support from Sumitomo Pharma Co., Ltd., Eisai Co., Ltd., Kyowa Kirin Co., Ltd.; grants from AMED, JSPS, and Ministry of Education Culture, Sports, Science and Technology Japan; and honoraria from Sumitomo Pharma Co., Ltd., Takeda Pharmaceutical Co., Ltd., Kyowa Kirin Co., Ltd., Ono Pharmaceutical Co., Ltd. S.O., H.T., N.U., K.I., and Y.H. has no financial disclosure.

References

1. McKeith IG, Dickson DW, Lowe J, et al. Diagnosis and management of dementia with Lewy bodies: third report of the DLB Consortium. Neurology 2005;65:1863-1872.
2. Beach TG, Adler CH, Lue L, et al. Unified staging system for Lewy body disorders: correlation with nigrostriatal degeneration, cognitive impairment and motor dysfunction. Acta Neuropathol 2009;117:613-634.
3. de Lau LM, Breteler MM. Epidemiology of Parkinson's disease. Lancet Neurol 2006;5:525-535.
4. Goedert M. Alpha-synuclein and neurodegenerative diseases. Nat Rev Neurosci

2001;2:492-501.
5. Kalia LV, Lang AE. Parkinson's disease. Lancet 2015;386:896-912.
6. Hely MA, Reid WG, Adena MA, Halliday GM, Morris JG. The Sydney multicenter study of Parkinson's disease: the inevitability of dementia at 20 years. Mov Disord 2008;23:837-844.
7. Braak H, Del Tredici K, Rub U, de Vos RA, Jansen Steur EN, Braak E. Staging of brain pathology related to sporadic Parkinson's disease. Neurobiol Aging 2003;24:197-211.
8. Braak H, de Vos RA, Bohl J, Del Tredici K. Gastric alpha-synuclein immunoreactive inclusions in Meissner's and Auerbach's plexuses in cases staged for Parkinson's disease-related brain pathology. Neurosci Lett 2006;396:67-72.
9. Li JY, Englund E, Holton JL, et al. Lewy bodies in grafted neurons in subjects with Parkinson's disease suggest host-to-graft disease propagation. Nat Med 2008;14:501-503.
10. Kordower JH, Chu Y, Hauser RA, Freeman TB, Olanow CW. Lewy body-like pathology in long-term embryonic nigral transplants in Parkinson's disease. Nat Med 2008;14:504-506.
11. Masuda-Suzukake M, Nonaka T, Hosokawa M, et al. Prion-like spreading of pathological alpha-synuclein in brain. Brain 2013;136:1128-1138.
12. Luk KC, Kehm VM, Zhang B, O'Brien P, Trojanowski JQ, Lee VM. Intracerebral inoculation of pathological alpha-synuclein initiates a rapidly progressive neurodegenerative alpha-synucleinopathy in mice. J Exp Med 2012;209:975-986.
13. Recasens A, Dehay B, Bove J, et al. Lewy body extracts from Parkinson disease brains trigger alpha-synuclein pathology and neurodegeneration in mice and monkeys. Ann Neurol 2014;75:351-362.
14. Uemura N, Ueda J, Yoshihara T, et al. α-Synuclein Spread from Olfactory Bulb Causes Hyposmia, Anxiety, and Memory Loss in BAC-SNCA Mice. Mov Disord 2021.
15. Uemura N, Uemura MT, Lo A, et al. Slow Progressive Accumulation of Oligodendroglial Alpha-Synuclein (alpha-Syn) Pathology in Synthetic alpha-Syn Fibril-Induced Mouse Models of Synucleinopathy. J Neuropathol Exp Neurol 2019;78:877-890.
16. Rey NL, Steiner JA, Maroof N, et al. Widespread transneuronal propagation of alpha-synucleinopathy triggered in olfactory bulb mimics prodromal Parkinson's disease. J Exp Med 2016;213:1759-1778.
17. Rey NL, George S, Steiner JA, et al. Spread of aggregates after olfactory bulb injection of alpha-synuclein fibrils is associated with early neuronal loss and is reduced long term. Acta Neuropathol 2018;135:65-83.
18. Hashikawa T, Nakatomi R, Iriki A. Current models of the marmoset brain. Neurosci Res 2015;93:116-127.
19. Ubeda-Bañon I, Saiz-Sanchez D, de la Rosa-Prieto C, Martinez-Marcos A. α-Synuclein in the olfactory system in Parkinson's disease: role of neural connections on spreading pathology. Brain Struct Funct 2014;219:1513-1526.
20. Okano H, Hikishima K, Iriki A, Sasaki E. The common marmoset as a novel animal model

460 system for biomedical and neuroscience research applications. Semin Fetal Neonatal Med
461 2012;17:336-340.
462 21. Sasaki E, Suemizu H, Shimada A, et al. Generation of transgenic non-human primates
463 with germline transmission. Nature 2009;459:523-527.
464 22. Shimozawa A, Ono M, Takahara D, et al. Propagation of pathological alpha-synuclein in
465 marmoset brain. Acta Neuropathol Commun 2017;5:12.
466 23. Uemura N, Yagi H, Uemura MT, Hatanaka Y, Yamakado H, Takahashi R. Inoculation of
467 alpha-synuclein preformed fibrils into the mouse gastrointestinal tract induces Lewy body-
468 like aggregates in the brainstem via the vagus nerve. Mol Neurodegener 2018;13:21.
469 24. Saito Y, Kawashima A, Ruberu NN, et al. Accumulation of phosphorylated alpha-synuclein
470 in aging human brain. J Neuropathol Exp Neurol 2003;62:644-654.
471 25. Luk KC, Covell DJ, Kehm VM, et al. Molecular and Biological Compatibility with Host
472 Alpha-Synuclein Influences Fibril Pathogenicity. Cell Rep 2016;16:3373-3387.
473 26. Shimozawa A, Ono M, Takahara D, et al. Propagation of pathological α-synuclein in
474 marmoset brain. Acta Neuropathol Commun 2017;5:12.
475 27. Massaad CA, Pautler RG. Manganese-enhanced magnetic resonance imaging (MEMRI).
476 Methods Mol Biol 2011;711:145-174.
477 28. Bourdenx M, Nioche A, Dovero S, et al. Identification of distinct pathological signatures
478 induced by patient-derived α-synuclein structures in nonhuman primates. Sci Adv
479 2020;6:eaaz9165.
480 29. Manfredsson FP, Luk KC, Benskey MJ, et al. Induction of alpha-synuclein pathology in the
481 enteric nervous system of the rat and non-human primate results in gastrointestinal
482 dysmotility and transient CNS pathology. Neurobiol Dis 2018;112:106-118.
483 30. Arotcarena ML, Dovero S, Prigent A, et al. Bidirectional gut-to-brain and brain-to-gut
484 propagation of synucleinopathy in non-human primates. Brain 2020.
485 31. Sengoku R, Saito Y, Ikemura M, et al. Incidence and extent of Lewy body-related alpha-
486 synucleinopathy in aging human olfactory bulb. J Neuropathol Exp Neurol 2008;67:1072-
487 1083.
488 32. Braak H, Braak E, Yilmazer D, et al. Amygdala pathology in Parkinson's disease. Acta
489 Neuropathol 1994;88:493-500.
490 33. McFadyen J. Investigating the Subcortical Route to the Amygdala Across Species and in
491 Disordered Fear Responses. J Exp Neurosci 2019;13:1179069519846445.
492 34. McGaugh JL, Roozendaal B. Drug enhancement of memory consolidation: historical
493 perspective and neurobiological implications. Psychopharmacology (Berl) 2009;202:3-14.
494 35. Ubeda-Banon I, Saiz-Sanchez D, de la Rosa-Prieto C, Martinez-Marcos A. alpha-Synuclein
495 in the olfactory system in Parkinson's disease: role of neural connections on spreading
496 pathology. Brain Struct Funct 2014;219:1513-1526.
497 36. Schapira AHV, Chaudhuri KR, Jenner P. Non-motor features of Parkinson disease. Nat

Rev Neurosci 2017;18:435-450.
37. Goldman JG, Stebbins GT, Bernard B, Stoub TR, Goetz CG, deToledo-Morrell L. Entorhinal cortex atrophy differentiates Parkinson's disease patients with and without dementia. Mov Disord 2012;27:727-734.
38. Van Den Berge N, Ferreira N, Mikkelsen TW, et al. Ageing promotes pathological alpha-synuclein propagation and autonomic dysfunction in wild-type rats. Brain 2021;144:1853-1868.
39. Wang J, You H, Liu JF, Ni DF, Zhang ZX, Guan J. Association of olfactory bulb volume and olfactory sulcus depth with olfactory function in patients with Parkinson disease. AJNR Am J Neuroradiol 2011;32:677-681.
40. Sengoku R, Matsushima S, Bono K, et al. Olfactory function combined with morphology distinguishes Parkinson's disease. Parkinsonism Relat Disord 2015;21:771-777.
41. McKeith IG, Boeve BF, Dickson DW, et al. Diagnosis and management of dementia with Lewy bodies: Fourth consensus report of the DLB Consortium. Neurology 2017;89:88-100.
42. Bohnen NI, Koeppe RA, Minoshima S, et al. Cerebral glucose metabolic features of Parkinson disease and incident dementia: longitudinal study. J Nucl Med 2011;52:848-855.
43. Baba T, Hosokai Y, Nishio Y, et al. Longitudinal study of cognitive and cerebral metabolic changes in Parkinson's disease. J Neurol Sci 2017;372:288-293.
44. Baba T, Kikuchi A, Hirayama K, et al. Severe olfactory dysfunction is a prodromal symptom of dementia associated with Parkinson's disease: a 3 year longitudinal study. Brain 2012;135:161-169.
45. Domellöf ME, Lundin KF, Edström M, Forsgren L. Olfactory dysfunction and dementia in newly diagnosed patients with Parkinson's disease. Parkinsonism Relat Disord 2017;38:41-47.
46. Fujishiro H, Nakamura S, Sato K, Iseki E. Prodromal dementia with Lewy bodies. Geriatr Gerontol Int 2015;15:817-826.
47. Roberts RF, Wade-Martins R, Alegre-Abarrategui J. Direct visualization of alpha-synuclein oligomers reveals previously undetected pathology in Parkinson's disease brain. Brain 2015;138:1642-1657.

Figure legends

FIG. 1. Phosphorylated-α-Syn (p-α-Syn) pathology of the OB in the unilaterally PFFs-inoculated marmoset and patients with Parkinson's disease (PD).

(A–F) Immunohistochemical staining of p-α-Syn (EP1536Y) in the OB of unilaterally PFFs-

inoculated marmoset at 3 months postinoculation (mpi). P-α-Syn inclusions were observed in the glomerular layer (GL), external plexiform layer (EPL), mitral cell layer (MCL), and granular cell layer (GCL) on the ipsilateral side **(A)**. Sparse p-α-Syn inclusions were observed on the contralateral side **(F)**. Red dashed-dotted lines indicate glomeruli. Scale bar: 100 μm **(A, F)**. Scale bar: 20 μm **(A–E)**. **(G)** A schematic illustration of the OB anatomy. Glomeruli (blue circle outline), periglomerular cells (magenta circle outline), tufted cells (green circle), mitral cells (green diamond), and granular cells (magenta small circle). **(H–N)** Immunohistochemical staining of p-α-Syn (EP1536Y) in the OB of two patients with PD (Patient 1 and Patient 2) and age matched control (Control 1). Scale bar: 50 μm **(H–J)**. Scale bar: 20 μm **(K–N)**.

FIG. 2. Immunostaining of p-α-Syn in the unilaterally PFFs-inoculated marmoset brain and the characterization of cell types harboring p-α-Syn inclusions.

(A) Coronal section at the level of the bregma +10.0 mm. Scale bar: 3 mm. Amygdala (Amy), piriform cortex (Piri), putamen (Pu), and caudate (Cau). **(B)** Immunohistochemical staining of p-α-Syn (EP1536Y) in the amygdala at 3 mpi. P-α-Syn-positive inclusions were observed in cell bodies (arrowheads) and neurites (arrow). Scale bar: 200 μm. Enlarged images are high-magnification image of a p-α-Syn-positive cytoplasmic inclusion and Lewy neurites-like deposition. Scale bar: 10 μm. **(C, D)** Immunohistochemical staining of p-α-Syn (81A and #64) showed p-α-Syn-positive cytoplasmic inclusions in the amygdala. Scale bar: 10 μm. **(E–G)** Double immunostaining of ubiquitin (Ub, green), p-α-Syn (#64, magenta) and DAPI (blue). Scale bar: 5 μm. **(H–J)** Double immunostaining of p62 (green), p-α-Syn (#64, magenta) and DAPI (blue). Scale bar: 5 μm. **(K–M)** Thioflavin S (ThS) staining (green) and immunostaining of p-α-Syn (81A, magenta), and DAPI (blue). Scale bar: 5 μm. **(N)** Double immunostaining of p-α-Syn (#64, magenta), NeuN (green), and DAPI (blue). Scale bar: 5 μm. **(O)** Double immunostaining of p-α-Syn (EP1536Y, magenta), GFAP (green), and DAPI (blue). Scale bar: 5 μm. **(P)** Double immunostaining of p-α-Syn (#64, magenta), Iba1 (green), and DAPI (blue). Scale bar 5: μm. **(Q)** Double immunostaining of p-α-Syn (EP1536Y, magenta), CNPase (green), and DAPI (blue). Scale bar: 5 μm. **(R–V)** Immunohistochemical staining of p-α-Syn

(EP1536Y) in the hippocampus at 6 mpi. Scale bar: 1000 μm **(R)**. Scale bar: 100 μm **(S–V)**. Cornu ammonis 1 (CA1), cornu ammonis 2 (CA2), cornu ammonis 3 (CA3), Dentate gyrus (DG). **(W)** Immunohistochemical staining of p-α-Syn (EP1536Y) of control 8 year-old marmoset (I3777). Scale bar: 3 mm. Enlarged image is high-magnification image of hippocampus. Scale bar: 50 μm.

FIG. 3. Immunohistochemical staining of p-α-Syn and heatmap in various brain regions of the unilaterally PFFs-inoculated marmosets at 3 mpi and 6 mpi.

(A, B) The representative images of p-α-Syn pathology of the unilaterally PFFs-inoculated marmosets at 3 and 6 mpi (H81 and I5937, respectively). The p-α-Syn pathology was more severe on the ipsilateral side in comparison to the contralateral side. **(C)** The distribution and severity of p-α-Syn pathology of four unilaterally PFFs-inoculated marmosets (H81 and I5924 at 3 mpi, I5937 and H82 at 6 mpi). The heatmap color scale presents the density of p-α-Syn pathology in each brain region of the unilaterally PFFs-inoculated marmosets. The density of p-α-Syn pathology from each marmoset was illustrated using a gradient color scale ranging from 0 to 10. Ipsilateral (Ip) and contralateral (Co). Scale bar: 100 μm. Anterior commissure (ac), nucleus accumbens (Acb), basolateral amygdala nucleus (AmyBL), central amygdala nucleus (AmyCe), cortical amygdala (AmyCo), lateral amygdala nucleus (AmyL), bed nucleus (Bed), globus pallidus (GP), inferior temporal cortex, anterior area (ITA), lateral olfactory tract (lo), primary motor cortex (M1), nucleus basalis of Meynert (NBM), perirhinal cortex (PRh), pulvinar nucleus (Pul), red nucleus (RN), septal nucleus (sept), substantia nigra pars reticulata (SNr), supraoptic hypothalamic nucleus (SO), superior temporal cortex, lateral area (STL), thalamus (Tha), olfactory tubercle (Tu).

FIG. 4. Measurements of the brain volume of the unilaterally PFFs-inoculated marmosets using manganese-enhanced MRI (MEMRI).

(A, B) Sagittal **(A)** and coronal **(B)** sections of a marmoset brain. The position of the coronal section (B) is indicated by the dashed line **(A)**. **(C)** An enlarged image of the OB. We analyzed five sections of each brain region in the unilaterally PFFs-inoculated marmosets at 3 mpi (n = 4). We measured the area and the intensity on the ipsilateral (PFFs-inoculated) and contralateral (PBS-inoculated) sides, as the OB is outlined **(C)**. **(D, E)** The volume or intensity ratios of ipsilateral (PFFs-inoculated) to contralateral (PBS-inoculated) side were shown in every brain region (**P < 0.01, paired t-test).

FIG. 5. The comparison of the p-α-Syn pathological change with cerebral glucose hypometabolism by ^{18}F-FDG PET on the unilaterally PFFs-inoculated marmosets.

(A, C) Flip-subtracted ^{18}F-FDG-PET images of two unilaterally PFFs-inoculated marmosets at 3 mpi (H81) and 6 mpi (I5937). The color scale bar indicates decreases of the standardized uptake value (SUV). See Methods section. **(B, D)** The severity of p-α-Syn pathology at 3 mpi (H81) and 6 mpi (I5937) is demonstrated using five different colors representing no pathology to very severe pathology, based on the semi-quantification scoring method described in Methods. Hippocampus (Hipp), primary visual cortex (V1), secondary visual area and visual area 4 (V4).

Supplementary FIG. S1. Inoculation of α-synuclein (α-Syn) preformed fibrils (PFFs) into the marmoset olfactory bulb (OB).

(A) Comparison of amino acid sequences between human (*Homo sapiens*) and marmoset (*Callithrix jacchus*) α-Syn (h-α-Syn and mar-α-Syn, respectively). Four amino acids differ between h-α-Syn and mar-α-Syn; these are highlighted in yellow. The epitopes of antibodies for α-Syn (Syn1) and phosphorylated α-Syn (pS129) used in this study are indicated in blue and red, respectively. **(B)** Coomassie brilliant blue (CBB) staining and Western blotting (WB) of mar-α-Syn monomer and fibrils. **(C)** The thioflavin T (ThT) assay. Fibrils show significantly high-intensity fluorescence at 535 nm (****$P < 0.0001$, $n = 3$, two-tailed unpaired Student's *t*-

test). **(D)** *In vitro* α-Syn fibrillization assay. A normalized ThT assay showed that the mixture of mar-α-Syn monomer and mar-α-Syn fibrils (Mar+MarF) induced fibrillization more rapidly than the mixture of mar-α-Syn monomer and h-α-Syn fibrils (Mar+HuF) (*$P < 0.05$, **$P < 0.01$, $n = 3$, two-tailed unpaired Student's *t*-test). **(E)** A CT/MRI fusion image of the marmoset head. **(F, G)** Surgical images of inoculation of α-Syn PFFs into the OB. Scale bar: 2 mm.

Supplementary FIG. S2. Proteinase K-resistance of p-α-Syn positive aggregates.
Immunohistochemical staining of p-α-Syn with or without proteinase K (ProK) at 3 and 6 mpi. Scale bar: 100 μm.

Supplementary FIG. S3. Immunohistochemical staining of Iba1 and GFAP.
Immunohistochemical staining of p-α-Syn, Iba1, and GFAP in the piriform cortex on ipsilateral and contralateral sides. Scale bar: 100 μm.

Supplementary FIG. S4. Immunohistochemical staining of tyrosine hydroxylase.
Immunohistochemical staining of tyrosine hydroxylase in substantia nigra pars compact (SNc) on ipsilateral and contralateral sides. Substantia nigra pars reticulata (SNr) and ventral tegmental area (VTA). Scale bar: 500 μm.

Supplementary FIG. S5. Immunohistochemical staining of single stranded DNA (ssDNA).
Immunohistochemical staining of ssDNA. Scale bar: 50 μm.

Supplementary FIG. S6. Original ^{18}F-FDG-PET images without flip-subtraction and MRI of marmosets after the inoculation of α-Syn PFFs.
(A, B) Original ^{18}F-FDG-PET images without flip-subtraction and MRI of two unilaterally PFFs-inoculated marmosets at 3 mpi (H81) and 6 mpi (I5937). The color scale bar indicates SUV. Frontal (Fro), temporal (Temp), parietal (Pari), and occipital lobi (Occi).

Supplementary Table S1. Experimental information of the marmosets.

The experimental information of unilaterally and bilaterally PFFs-inoculated marmosets.

Supplementary Table S2. Pathological stages and clinical information of the patients with PD and a control subject.

The pathological stages and clinical data of two patients, who were clinically diagnosed as PD, and control subjects. Braak NFT stage (silver staining and AT8) are described as (right/left side) in Supplementary Table S2.

Supplementary Methods

Preparation of marmoset α-Syn expressing plasmid

The marmoset α-Syn (mar-α-Syn) messenger RNA (mRNA) was purified from a frozen marmoset brain sample, and mar-α-Syn complementary DNA (cDNA) was produced via reverse transcription. Primers 5'-ATGGATGTATTCATGAAAGGACTT-3' and 3'-CTGCTGACAGACGTTCCATCC-5' were used to amplify the mar-α-Syn cDNA with NdeI and HindIII restriction sites. Amplified DNA was cloned into the plasmid pRK172 between the NdeI and HindIII restriction sites and expressed in *Escherichia coli* BL21 (DE3) (BioDynamics Laboratory).

Preparation of recombinant α-Syn and PFFs

Purified α-Syn (7 mg/ml) was incubated at 37 °C in a shaking incubator at 1,000 rpm in 30 mM Tris–HCl buffer, pH 7.5, containing 150 mM KCl, for 120 hrs. α-Syn PFFs were pelleted by ultracentrifugation at 186,000 ×g for 20 min, resuspended in phosphate-buffered saline (PBS) (4 mg/ml), and sonicated for 2.5 min (Cosmo Bio, Bioruptor) before use. The protein concentrations were determined by BCA Protein Assay kit (Thermo Fisher).

In vitro α-Syn fibrillization assay

The reaction buffer was composed of PBS, 5 μM thioflavin T (ThT) (Sigma-Aldrich, #T3516), and 2 mg/ml recombinant mar-α-Syn monomer. Each well of a black 96-well plate (Costar) contained 100 μl reaction buffer, which was seeded with 1% (w/v) mar-α-Syn or h-α-Syn PFFs. The plates were sealed with a plate sealer film (4titude, qPCR seal) and incubated in a multi-label plate reader (PerkinElmer, 2030 ARVO X) at 37°C for 14 hrs with continuous shaking at 900 rpm. ThT fluorescence measurements (450 nm excitation and 535 nm emission) were taken every 30 min. These data were normalized between 0 and 100.

Sodium dodecyl sulfate (SDS)-polyacrylamide gel electrophoresis (PAGE) and western blot analysis

For SDS-PAGE, sample buffer (1% [w/v] SDS, 12.5% [w/v] glycerol, 0.005% [w/v] bromophenol blue, 2.5% [v/v] 2-mercaptoethanol, 25 mM Tris-HCl, pH 6.8) was added to mar-α-Syn monomer solution or the mar-α-Syn PFFs pellet, which was resuspended by vortex. Samples containing 10 μg protein were run on SuperSep™ Ace 5%–20% (Wako) and stained with Coomassie Brilliant Blue (CBB), or electrophoretically transferred to polyvinylidene difluoride membranes. For immunoblotting, the membranes were incubated with 4% (w/v) paraformaldehyde (PFA) in PBS for 30 min at room temperature to prevent detachment of α-Syn from the blotted membranes and then blocked with 5% (w/v) skim milk in PBS. The membranes were incubated with an anti-α-Syn primary antibody (Bioscience BD610787 [Syn1], 1:1000) at 4°C overnight. The membranes were incubated for 1 hr at room temperature with a horseradish peroxidase secondary antibody (Santa Cruz #sc-2005, 1:5000), and the protein bands were visualized using Chemi-Lumi One Super (nacalai tesque). Chemiluminescent signal was detected using an Amersham Imager 600 imager (GE Healthcare).

Animals

Four marmosets, two males at two years old (H81 and H82; born at the Bioresource Center, Gunma University Graduate School of Medicine) and two females at two years old (I5937 and I5924; born at CLEA Japan, Inc.) were used for α-Syn PFFs inoculation into the unilateral OB. Additionally, one female at eight years old (I3777; born at CLEA Japan, Inc.) was used for the immunohistochemical control. All experimental procedures were performed in accordance with the National Institutes of Health Guidelines for the Care and Use of Laboratory Animals and Basic Policies for the Conduct of Animals Experiments in Research Institutions by MEXT, Japan. Approval was obtained from the Animal Research Committee of Kyoto University (MedKyo 16,651) and Hamamatsu Photonics K.K. (HPK-2018-06).

Inoculation with α-Syn PFFs into the OB

We performed MRI before inoculation with mar-α-Syn PFFs (see Methods). Anesthesia was induced by intramuscular injections of ketamine hydrochloride (Ketalar, 30 mg/kg, Daiichi Sankyo, Tokyo, Japan), and atropine sulfate (0.1 mg, i.m.) and isoflurane (1%–1.5%) was administered by inhalation to maintain anesthesia throughout surgery. Ampicillin (40 mg/kg) was injected as an antibiotic before surgery and ketoprofen (0.4 mg/kg) was administered to reduce postoperative pain and inflammation after surgery. Under anesthesia, the head of the marmoset was fixed to the stereotaxic apparatus and the operation was performed. Heart rate, O_2 saturation, and body temperature were continuously monitored. A glass capillary (tip diameter, 80–100 μm) was filled with the α-Syn PFFs solution, which was mixed with green dye, fast green FCF (final concentration 0.02%, nacalai), to visualize the leak. For the unilateral PFFs inoculation, 0.8 μl of 4 mg/ml α-Syn PFFs was stereotactically injected into the two sites of the unilateral OB (a total of 1.6 μl) (AP, +1.00 mm; L, −0.90 mm; D, 1.50 mm and AP, +1.50mm; L, −0.90 mm; D, 1.0 mm relative to the border between OB-cerebrum and dural surface) at a constant rate of 0.1 μl per minute controlled by a syringe pump (Legato 130, KD Scientific). The same volume of PBS was also injected into the contralateral OB. After inoculation, the glass capillary was left in place for 5 min to prevent leakage of the injected solution. No leakage was observed after the glass capillary was pulled out. The dura

was covered with dental resign and the skin was closed with suture. After the operation, ampicillin (40 mg/kg) and diclofenac (Voltaren, 10 mg) were administered intramuscularly.

Preparation of histological analysis for the marmosets

At 3 or 6 months postinoculation (mpi), the unilaterally PFFs-inoculated marmosets were deeply anesthetized with an intramuscular injection of ketamine, and given an intraperitoneal injection of sodium pentobarbital (more than 35 mg/kg). They were then transcardially perfused with PBS followed by 4% (w/v) paraformaldehyde in PBS (pH 7.4). The brains were removed and immersed in 4% (w/v) PFA in PBS overnight. They were dehydrated and embedded in paraffin, and 8-μm thick paraffin sections were prepared with a HM 325 rotary microtome (MICROM).

Immunohistostaining

The following primary antibodies were used for immunohistostaining analysis: anti-phosphorylated-α-Syn (p-α-Syn) (Abcam, #ab51253 [EP1536Y], 1:5000), anti-p-α-Syn (Wako, #015-25191 [#64], 1:2000), anti-p-α-Syn (Abcam, #ab184674 [81A], 1:5000), anti-p62 (MBL, #PM045, 1:1000), anti-ubiquitin (DAKO, #Z0458, 1:500), anti-NeuN (Millipore, ABN78, 1:400), anti-GFAP (Invitrogen, #130300, 1:200), anti-Iba1 (Wako, 019-19741, 1:200), single stranded DNA (ssDNA) (DAKO, #A4506, 1:2000), anti-TH (Millipore, #MAB318, 1:1000), and anti-CNPase (Millipore, MAB326, 1:500). The sections were incubated at 4 °C with primary antibodies overnight and then processed for visualization. As secondary antibodies, Histofine (Nichirei Bioscience) was used for diaminobenzidine (DAB) staining, and Alexa Fluor 488 or 594-conjugated antibodies (Molecular Probes) for immunofluorescence. Sections were examined using a BX43 microscope (Olympus), a BZ-X710 fluorescence microscope (KEYENCE), and an FV-1000 confocal laser scanning microscope (Olympus).

Thioflavin S staining

For p-α-Syn and thioflavin S (ThS, SantaCruz, #sc-391005) double-labeling staining,

after immunolabeling with p-α-Syn antibody, sections were incubated with 0.05% ThS in 50% ethanol followed by differentiation with 80% ethanol. Sections were examined with an FV-1000 confocal laser scanning microscope (Olympus).

Proteinase K-resistance

To assess proteinase K-resistant phosphorylated α-Syn, the tissue was treated by 20 μg/ml proteinase K (nacalai tesque, Kyoto, Japan) in PBS for 30 min at room temperature after antigen retrieval.

Heatmap and scoring of p-α-Syn pathology

We assessed the p-α-Syn pathology density in various brain regions using quantitative methods modified from a previous report.[1] We randomly took a total of three images from three sections for each brain region at 20× magnification using a BZ-X710 fluorescence microscope (KEYENCE). To generate a heatmap, we separated the DAB channel from the hematoxylin channel using ImageJ, converted the processed images to 8-bit data, measured the density of these images for quantification of the p-α-Syn-positive area, and then averaged the density of three images for each brain region to minimize bias. We presented the data on a heatmap programmed using Excel 2007 software (Microsoft).

We also assessed the severity of p-α-Syn pathology in a semi-quantitative way, based on the previous reports,[1,2] in the same coronal sections as those shown by positron emission tomography (PET) images (FIG. 5). We determined the severity using a score system, from no pathology to very severe pathology at 20× magnification (no pathology = no neuritic pathology and 0 inclusion, mild pathology = neuritic pathology or 0–2 inclusions, moderate pathology = 3–9 inclusions, severe pathology = 10–20 inclusions, very severe pathology = more than 20 inclusions per field).

Manganese-Enhanced MRI (MEMRI)

To enhance the intensity of MR signals of neural activity in the marmoset brain, we performed MEMRI by administrating $MnCl_2$ (25 mg/kg, i.p.) two times in 48 hrs intervals. 24 hrs after the last $MnCl_2$ injection MRI was performed using a 3T MRI scanner (Verio, Siemens, USA) under 1.5% isoflurane anesthesia. A custom-built 16-ch helmet-type radiofrequency coil with a 12 cm inner diameter was used for reception (Takashima seisakusho Co., Ltd, Japan). High resolution 3D T1-weighted imaging was performed with a 3D fast spin-echo with two echoes (TE = 11 ms, TR = 150 ms, FOV = 50×50×50 mm, Matrix = 192×192×192, Number of averages = 4). We assessed the volume and intensity of MEMRI on the OB, frontal lobe, temporal lobe, and occipital lobe. We outlined five sections per these regions, and measured the area and the intensity of these regions using ImageJ software. We then calculated the volume or intensity ratio of ipsilateral to contralateral side every region in unilaterally PFFs-inoculated marmosets. Volume ratio was calculated as $\sum_{i=1}^{5}(Vi \times Hi) \ / \ \sum_{i=1}^{5}(Vi' \times Hi')$. V and V' means area of the targeted brain regions on ipsilateral or contralateral side, respectively. H and H' means height of the targeted brain regions on ipsilateral or contralateral side, respectively. Intensity ratio was also calculated as $\sum_{i=1}^{5}(Ii \times Hi) \ / \ \sum_{i=1}^{5}(Ii' \times Hi')$. I and I' means intensity of the targeted brain regions on ipsilateral or contralateral side, respectively. Paired t-test was used for the statistical analysis.

PET imaging

To measure regional cerebral glucose utilization (rCGU) as an index of neural activity, PET imaging using ^{18}F-fluoro-2-deoxy-D-glucose (^{18}F-FDG) was performed using PET scanner (SHR-38000, Hamamatsu Photonics K.K., Japan).

To avoid the anesthetic effects on rCGU, ^{18}F-FDG was injected via a cannulated tail vein while the marmosets were awake outside the PET scanner, followed by permitting them to freely move in the cage. 30 min after the injection, the animal was rapidly anesthetized by 1.5 % isoflurane via face mask, placed on the PET scanner using a stereotactic head holder, and dynamic emission scan was performed for 120 min. Transmission data scan for attenuation correction were acquired for 30 min on a different day. Marmosets had a bolus injection of ^{18}F-

FDG averaging 94.75 MBq/body.

PET data analysis

Reconstruction was performed using an iterative 3-D dynamic raw-action maximum likelihood algorithm (3D-DRAMA) (Tanaka and Kudo, 2010) with a Gaussian filter of 1.0 mm in full width at half maximum (FWHM).

The summated ^{18}F-FDG images were used for further quantitative analysis of rCGU. The index of ^{18}F-FDG uptake is shown as a standardized uptake value (SUV), SUV = radioactivity concentration (Bq/cm^3)/injected radioactivity (Bq) × body weight (g), and values were converted to the global mean ratio by scaling whole-brain SUVs. The reconstructed PET images (pixel size 0.65 × 0.65 × 1.0167 mm) were realigned and co-registered with each subject's MRI using PMOD version 3.7 (PMOD Technologies, Zurich, Switzerland), and were spatially normalized to the Marmoset MRI Standard Brain (https://brainatlas.brain.riken.jp/marmoset/modules/xoonips/listitem.php?index_id=71) by applying the transformation matrix obtained by individual MRI. The index of ^{18}F-FDG uptake ratio normalized in brain tissues is shown as standardized uptake value (SUV): SUV=tissue radioactivity concentration (MBq/cc)/injected radioactivity (MBq)×body weight (g).

To identify the changes in rCGU after the inoculation, original ^{18}F-FDG-PET images were flipped horizontally, and were subjected to a voxel-based subtraction from the flipped images comparing the affected and unaffected brain hemispheres. All images were visualized with MRIcroGL software (https://www.nitrc.org/projects/mricrogl).

Reference

1. Rey NL, Steiner JA, Maroof N, et al. Widespread transneuronal propagation of alpha-synucleinopathy triggered in olfactory bulb mimics prodromal Parkinson's disease. J Exp Med 2016;213:1759-1778.
2. Rey NL, George S, Steiner JA, et al. Spread of aggregates after olfactory bulb injection of alpha-synuclein fibrils is associated with early neuronal loss and is reduced long term.

Acta Neuropathol 2018;135:65-83.

Supplementary Table S1

The experimental information of unilaterally and bilaterally PFFs-inoculated marmosets.

Unilaterally PFFs-inoculated	MEMRI 3 mpi	^{18}F-FDG-PET 3 mpi	^{18}F-FDG-PET 6 mpi	Pathological analysis
H81	✓	✓	n.a.	3 mpi
I5924	✓	n.a.	n.a.	3 mpi
I5937	✓	n.a.	✓	6 mpi
H82	✓	n.a.	n.a.	6 mpi

Supplementary Table S2

Subjects	Age	Sex	Hoehn &	Braak PD	BBAR	Senile	Braak Stage	Braak Stage	Post mortem
Patient 1	87	M	5	4	6	1	3/3	3/3	05:53:00
Patient 2	75	M	4	3	4	1	3/2	3/2	54:20:00
Control 1	83	M	0	0	0	0	1/2	1/2	03:55:00

FIG. 1.

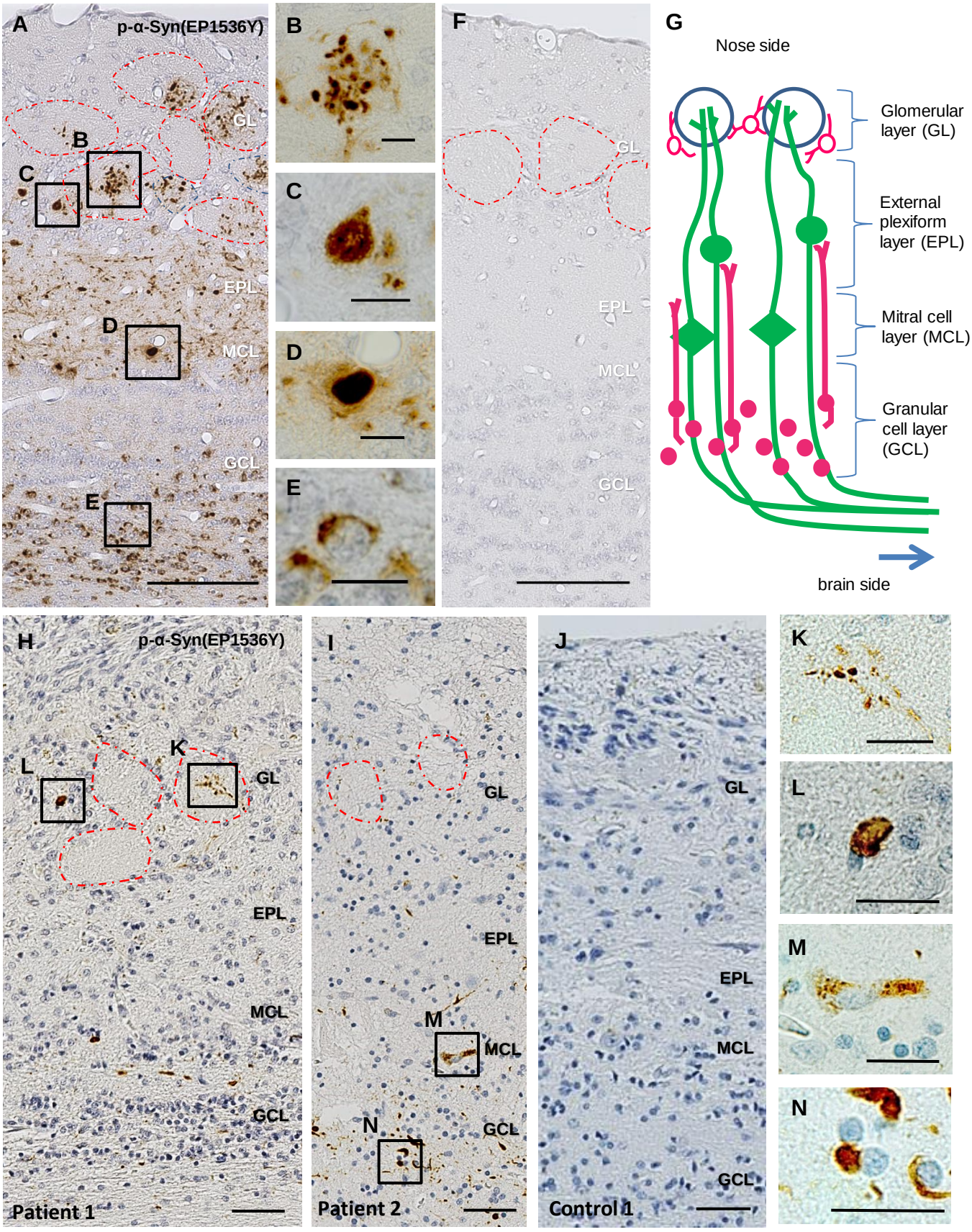
A
p-α-Syn(EP1536Y)
GL
B
C
EPL
D
MCL
GCL
E
B
C
D
E
F
GL
EPL
MCL
GCL
G
Nose side
Glomerular layer (GL)
External plexiform layer (EPL)
Mitral cell layer (MCL)
Granular cell layer (GCL)
brain side
H
p-α-Syn(EP1536Y)
L
K
GL
EPL
MCL
GCL
Patient 1
I
GL
EPL
M
MCL
N
GCL
Patient 2
J
GL
EPL
MCL
GCL
Control 1
K
L
M
N

FIG. 2.

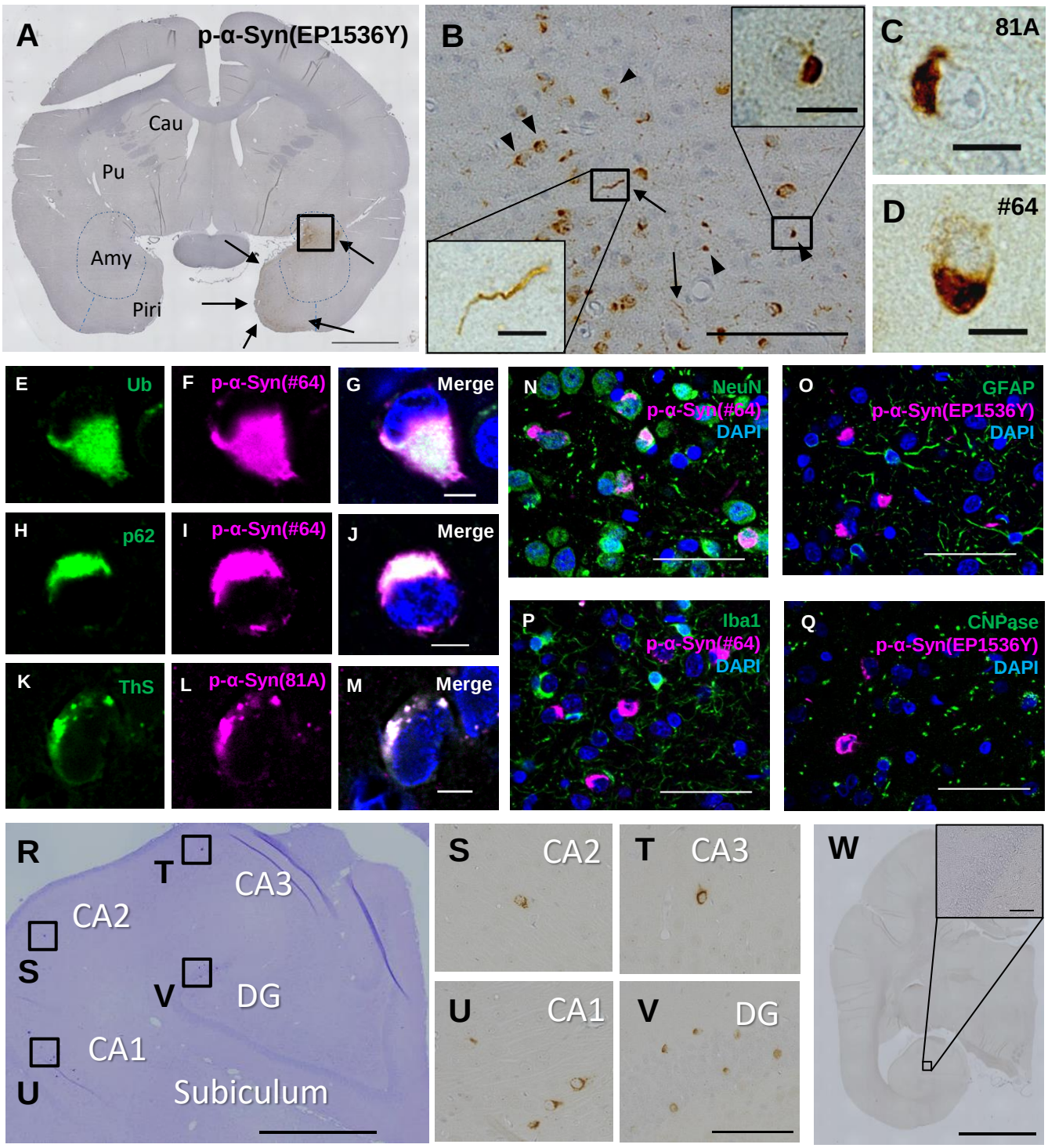
A
p-α-Syn(EP1536Y)
Cau
Pu
Amy
Piri
B
C
81A
D
#64
E
Ub
F
p-α-Syn(#64)
G
Merge
H
p62
I
p-α-Syn(#64)
J
Merge
K
ThS
L
p-α-Syn(81A)
M
Merge
N
NeuN
p-α-Syn(#64)
DAPI
O
GFAP
p-α-Syn(EP1536Y)
DAPI
P
Iba1
p-α-Syn(#64)
DAPI
Q
CNPase
p-α-Syn(EP1536Y)
DAPI
R
T
CA3
CA2
S
V
DG
CA1
U
Subiculum
S
CA2
T
CA3
U
CA1
V
DG
W

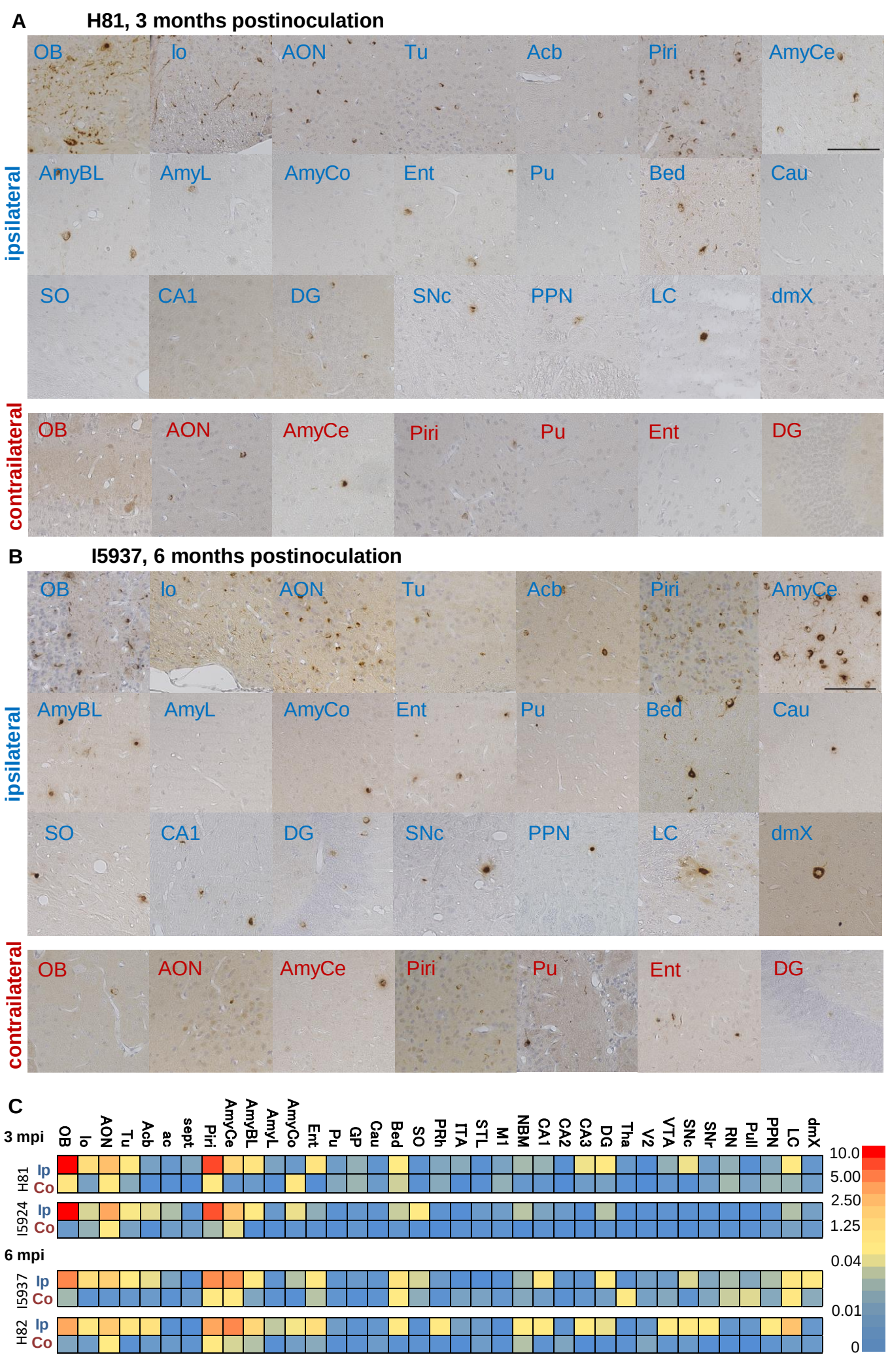
A
H81, 3 months postinoculation
ipsilateral
OB
Io
AON
Tu
Acb
Piri
AmyCe
AmyBL
AmyL
AmyCo
Ent
Pu
Bed
Cau
SO
CA1
DG
SNc
PPN
LC
dmX
contrailateral
OB
AON
AmyCe
Piri
Pu
Ent
DG
B
I5937, 6 months postinoculation
ipsilateral
OB
Io
AON
Tu
Acb
Piri
AmyCe
AmyBL
AmyL
AmyCo
Ent
Pu
Bed
Cau
SO
CA1
DG
SNc
PPN
LC
dmX
contrailateral
OB
AON
AmyCe
Piri
Pu
Ent
DG
C
3 mpi
OB
Io
AON
Tu
Acb
ac
sept
Piri
AmyCe
AmyBL
AmyL
AmyCo
Ent
Pu
GP
Cau
Bed
SO
PRh
ITA
STL
M1
NBM
CA1
CA2
CA3
DG
Tha
V2
VTA
SNc
SNr
RN
Pull
PPN
LC
dmX
H81
Ip
Co
I5924
Ip
Co
6 mpi
I5937
Ip
Co
H82
Ip
Co
10.0
5.00
2.50
1.25
0.04
0.01
0

FIG. 4.

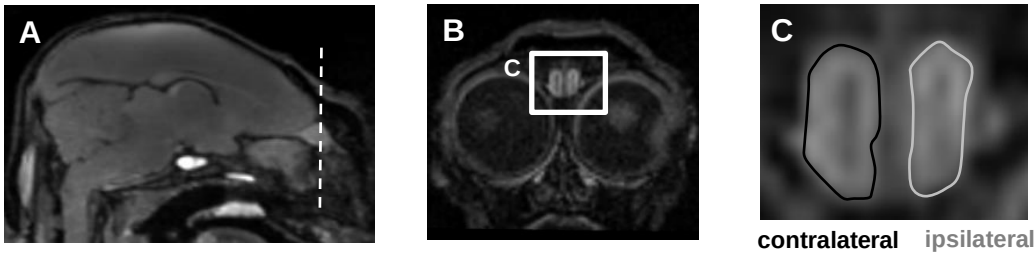
A
B
C
C
contralateral
ipsilateral

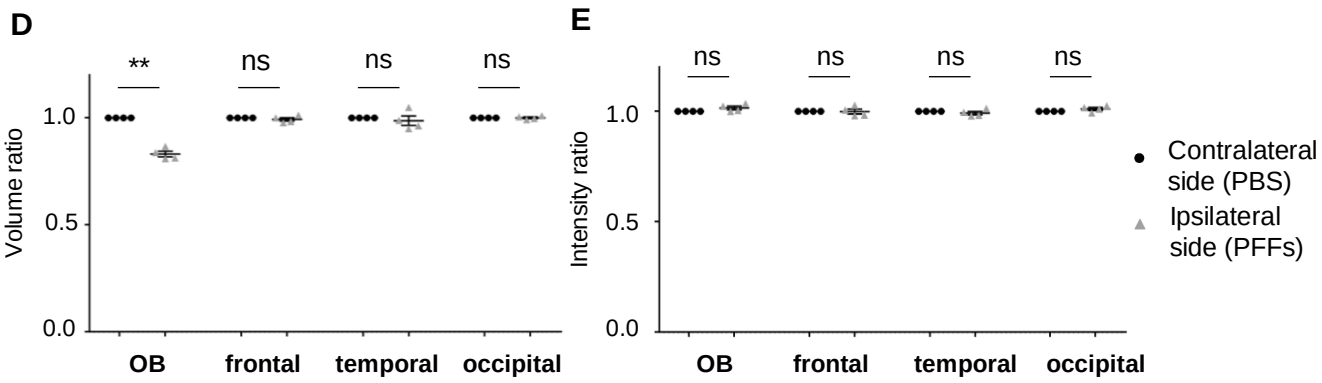
D
**
ns
ns
ns
Volume ratio
1.0
0.5
0.0
OB
frontal
temporal
occipital
E
ns
ns
ns
ns
Intensity ratio
1.0
0.5
0.0
OB
frontal
temporal
occipital
Contralateral side (PBS)
Ipsilateral side (PFFs)

FIG. 5.

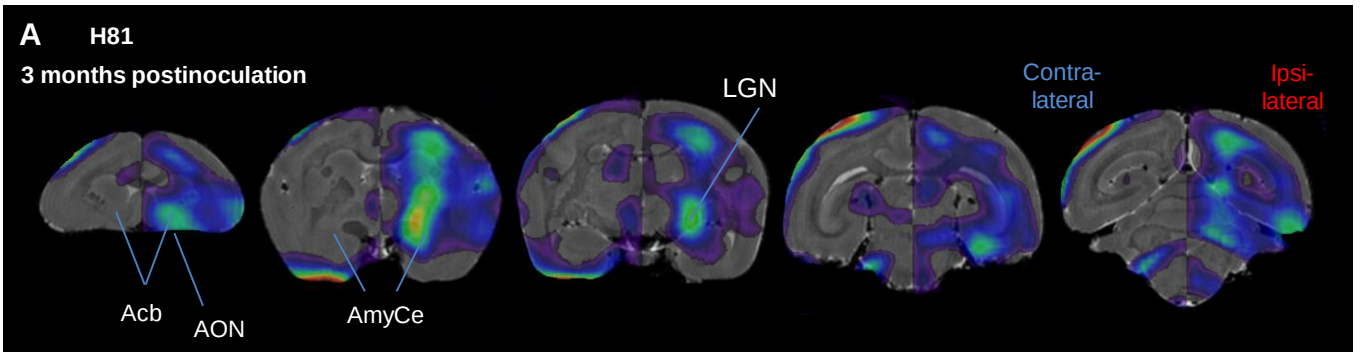
A
H81
3 months postinoculation
LGN
Contra-
lateral
Ipsi-
lateral
Acb
AON
AmyCe

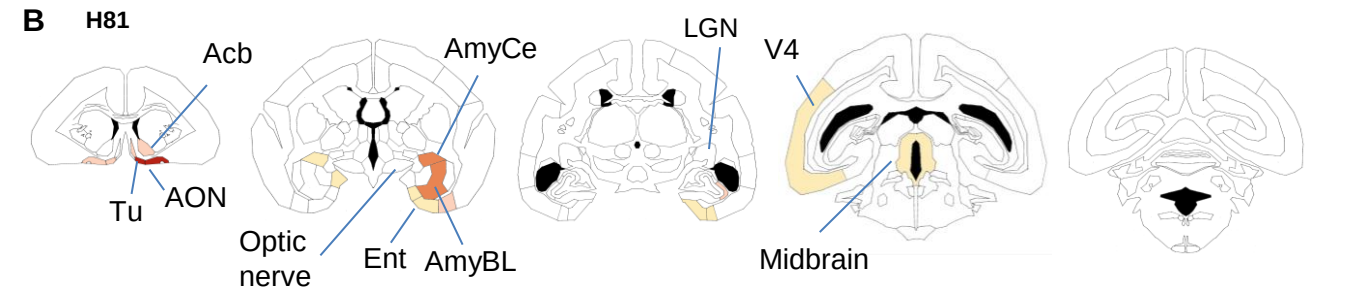
B
H81
Acb
AmyCe
LGN
V4
Tu
AON
Optic
nerve
Ent
AmyBL
Midbrain

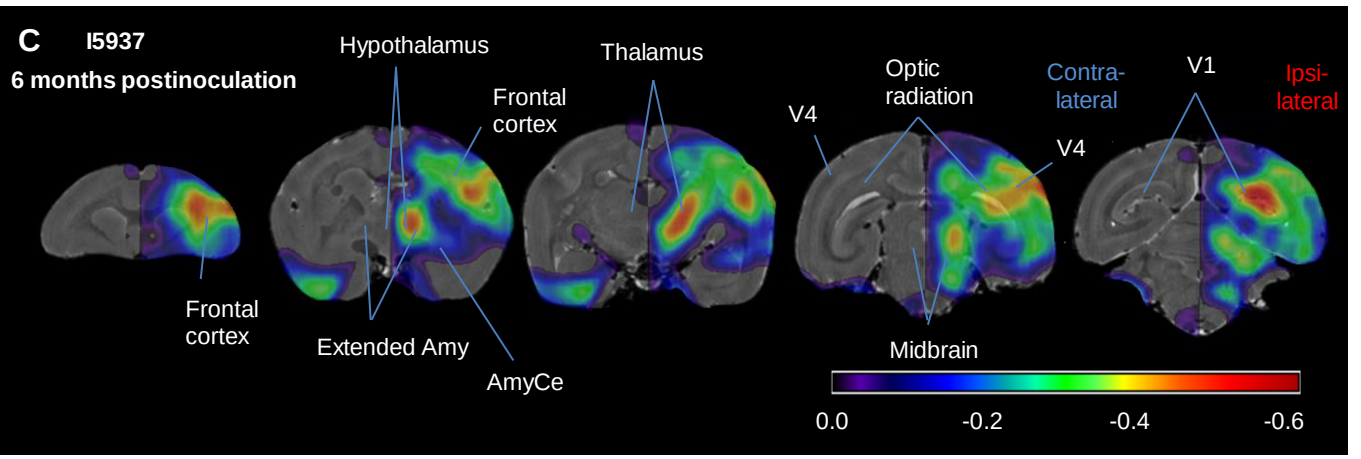
C
I5937
6 months postinoculation
Hypothalamus
Thalamus
Frontal
cortex
Optic
radiation
Contra-
lateral
V1
Ipsi-
lateral
V4
V4
Frontal
cortex
Extended Amy
AmyCe
Midbrain
0.0
-0.2
-0.4
-0.6

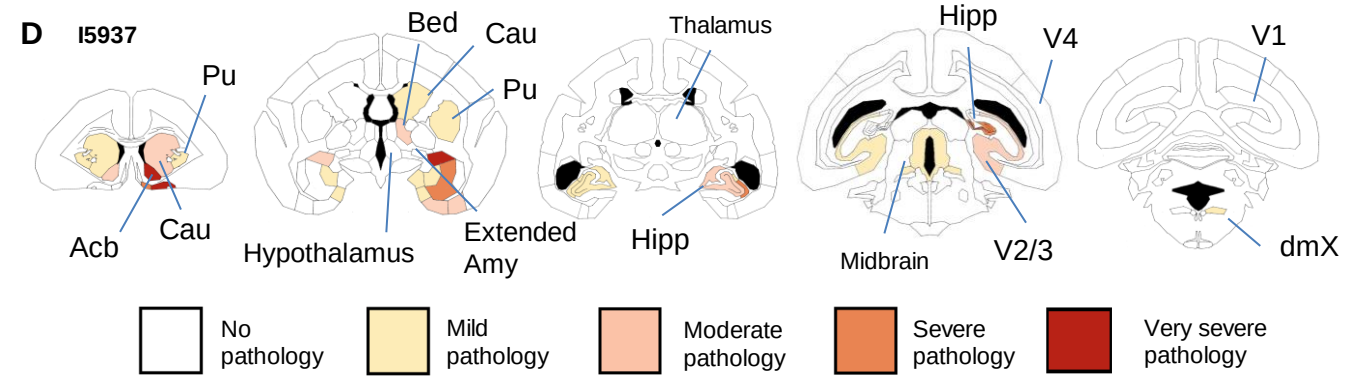
D
I5937
Bed
Cau
Pu
Thalamus
Hipp
V4
V1
Pu
Acb
Cau
Hypothalamus
Extended
Amy
Hipp
Midbrain
V2/3
dmX
No
pathology
Mild
pathology
Moderate
pathology
Severe
pathology
Very severe
pathology

Supplementary FIG. S1.

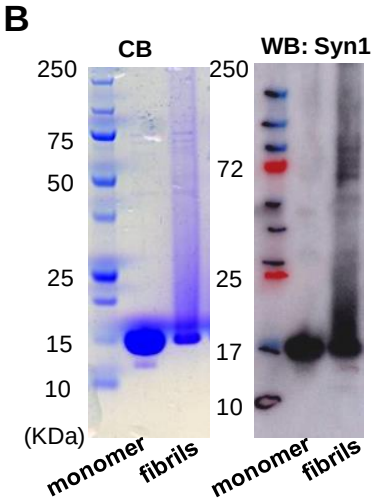

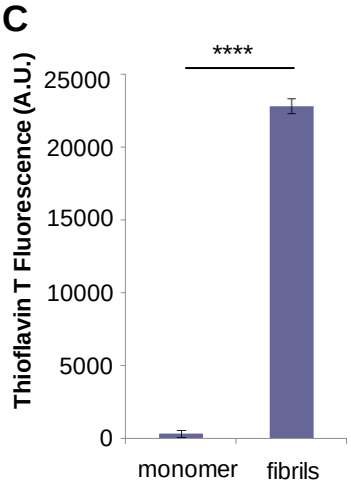

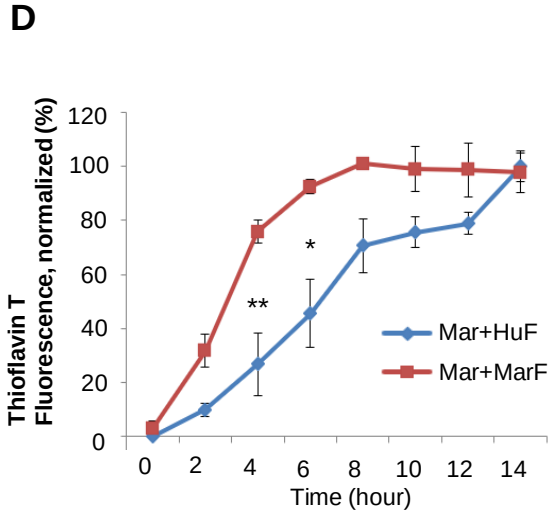

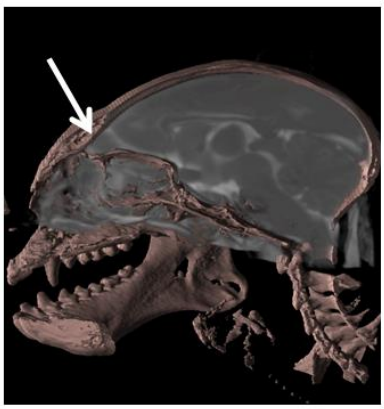

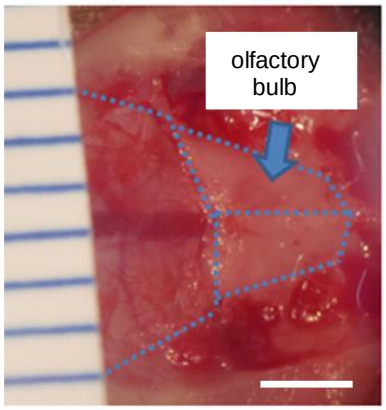

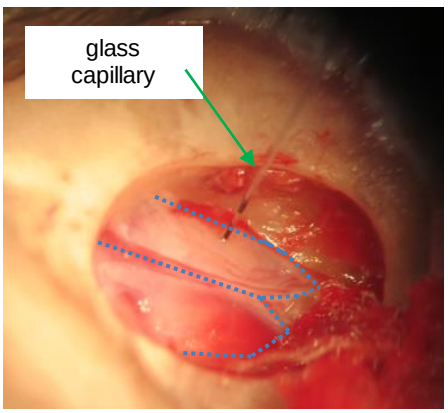

Supplementary FIG. S2.

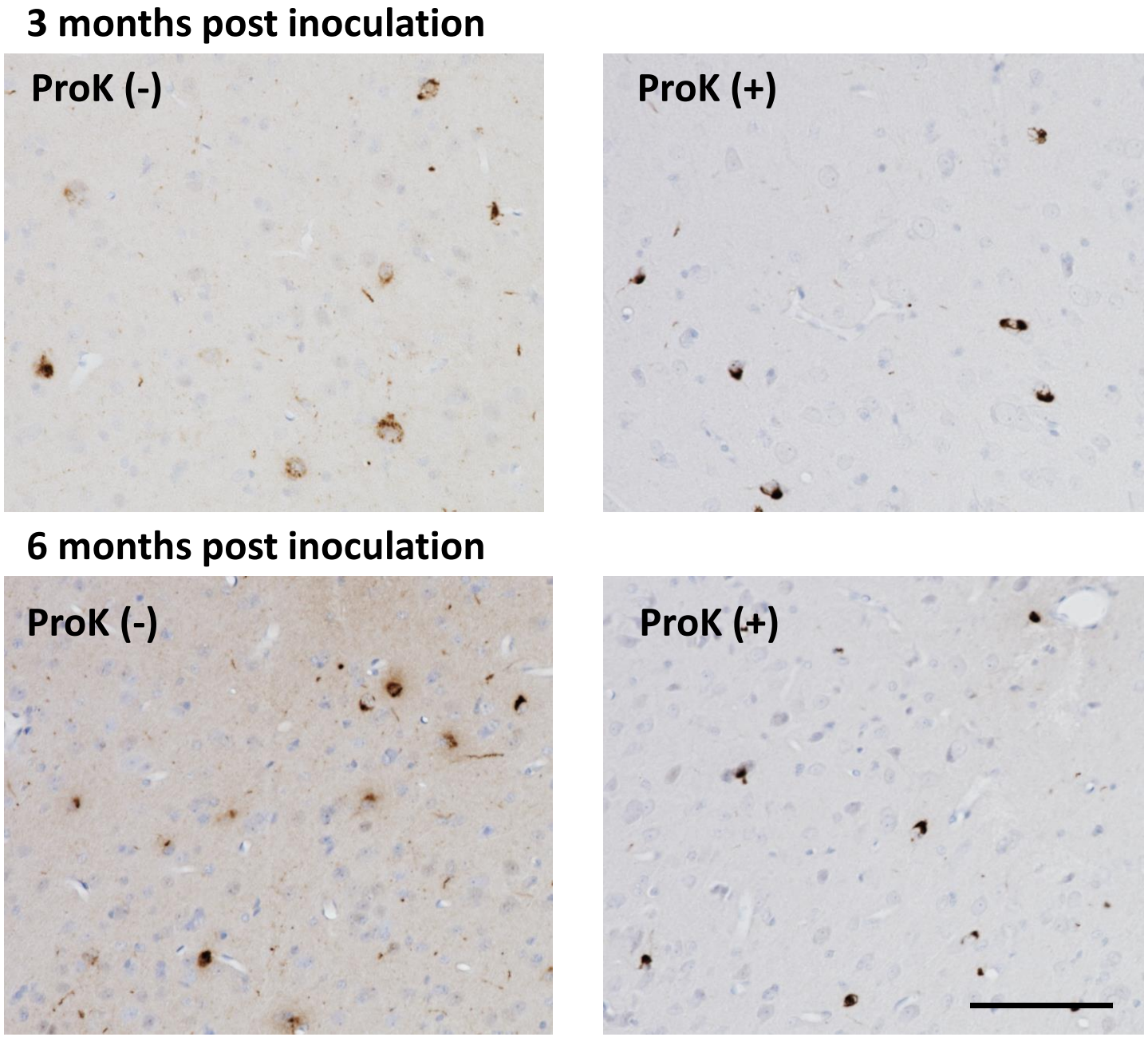

Supplementary FIG. S3.

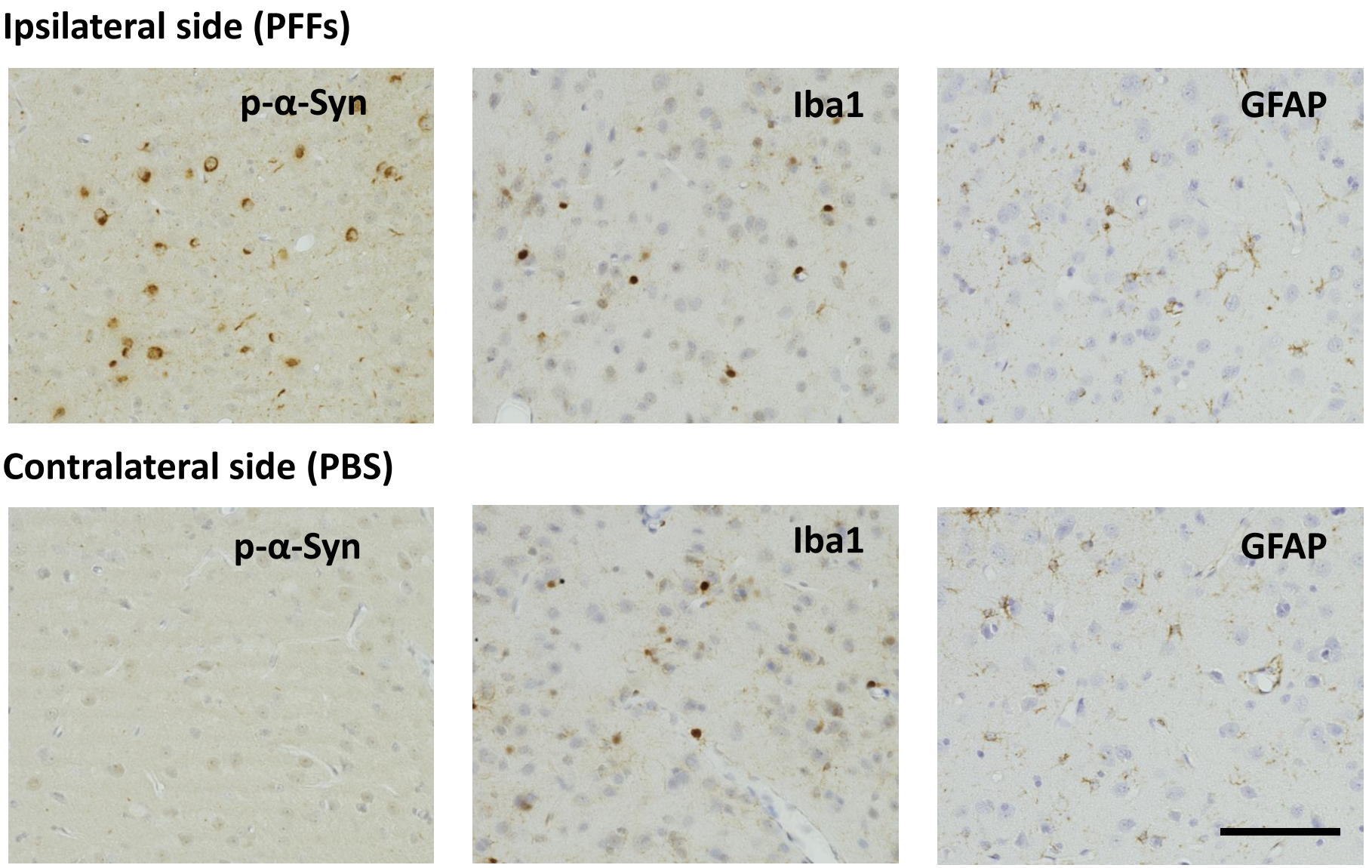

Supplementary FIG. S4.

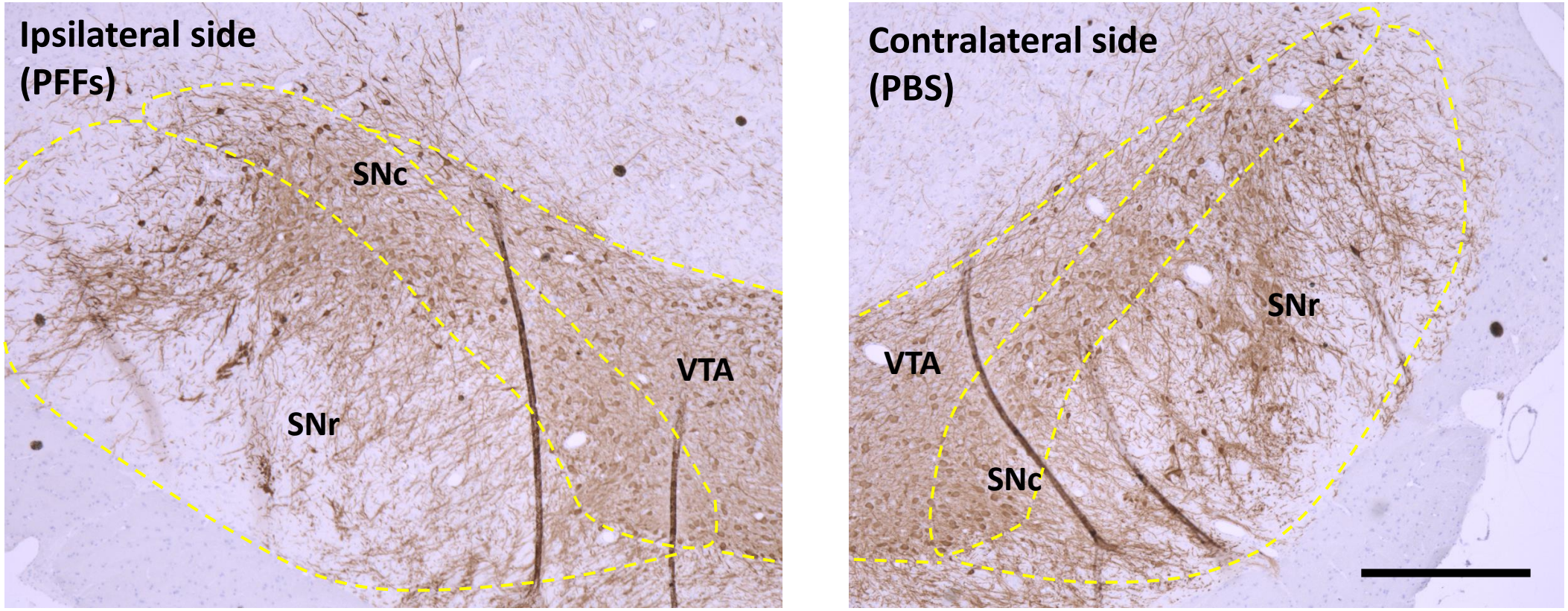

Supplementary FIG. S5.

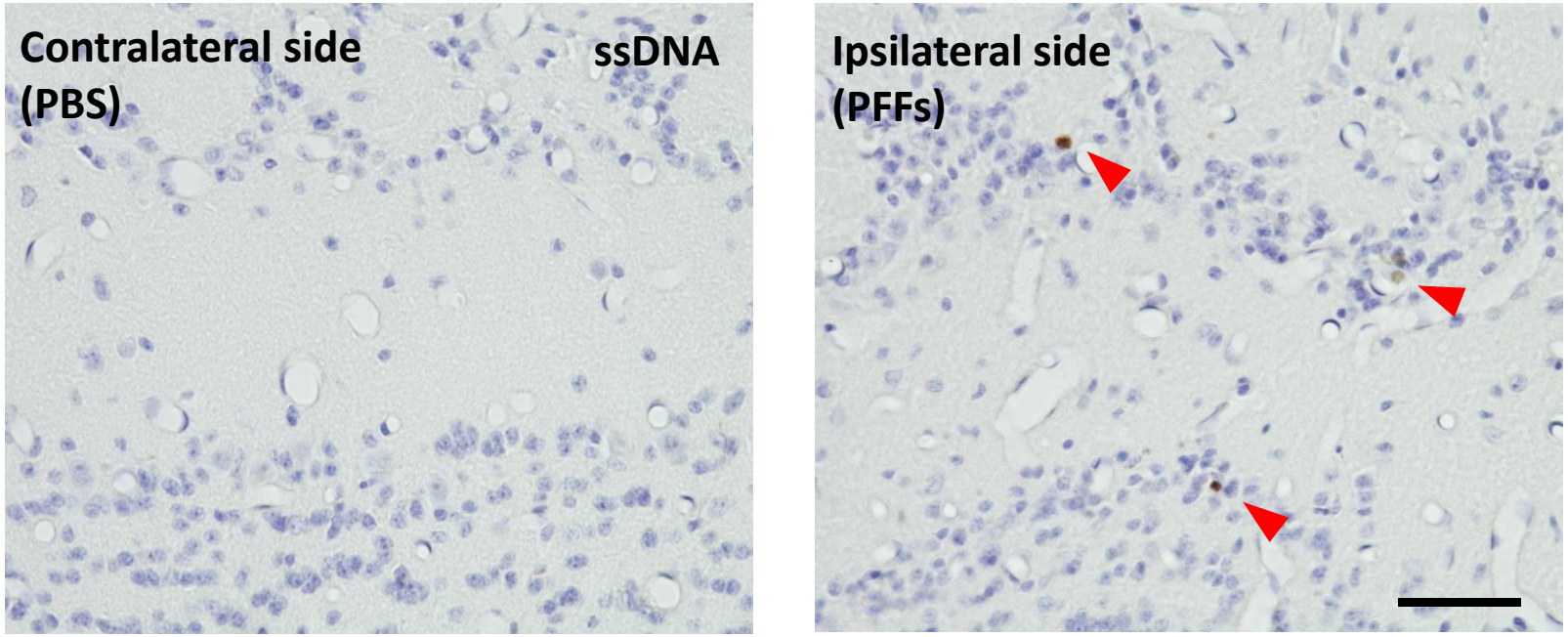

Supplementary FIG. S6.